A version of the Cloude/van Zyl decomposition for full/quad pol synthetic aperture radar data

Nielsen, Allan Aasbjerg; Connetable, Paul Jacques; Skriver, Henning; Conradsen, Knut

Link to article, DOI:
10.11581/dtu.00000237

Publication date:
2022

Document Version
Publisher's PDF, also known as Version of record

A version of the Cloude/van Zyl decomposition for full/quad pol synthetic aperture radar data

Allan Aasbjerg Nielsen[a], Paul Jacques Connetable[b], Henning Skriver[b] and Knut Conradsen[a]

[a]DTU Compute – Applied Mathematics and Computer Science, Building 324
[b]DTU Space – National Space Institute, Building 348
Technical University of Denmark, DK-2800 Lyngby, Denmark

ARTICLE HISTORY
Compiled April 8, 2022

ABSTRACT
Based on the Cloude/van Zyl decomposition of reflection symmetric polarimetric SAR data we present a version for full/quad polarisation data. We demonstrate both versions on X-band F-SAR data over Vejers, Denmark. Differences between the original and our version of the decomposition occur especially for very bright man-made targets. These differences come with lower entropy for our version giving an improved focus on a more pronounced dominant scattering mechanism for these objects. Interpretation of the scattering mechanism related to the full/quad pol version of the decomposition is facilitated by means of the Cloude/Pottier $\bar{\alpha}$ angle.

KEYWORDS
Complex covariance matrices, Hermitian matrices, polarimetric SAR.

1. Introduction

In (van Zyl 1993) van Zyl describes what he calls the Cloude decomposition (Cloude 1992) for polarimetric synthetic aperture radar (SAR) data. The Cloude decomposition is the general spectral decomposition consisting of sums of products of eigenvalues (sorted non-increasingly) and outer products of the corresponding eigenvectors of the Hermitian 3×3 covariance matrix of multilook SAR data. In (van Zyl et al. 2011) which deals primarily with another subject, namely an improvement of the Freeman/Durden decomposition (Freeman and Durden 1998), the decomposition in (van Zyl 1993) for reflection symmetric data is described further with an explicit distinction between single and double bounce (dihedral) targets. Inspired by this work we here give a version of the decomposition for full/quad pol SAR data.

For both the original, reflection symmetry and the full/quad pol versions of the decomposition, the eigenvalues needed are calculated by means of fast methods described in (Uspensky 1948; Nielsen 2020).

Shortcomings in the van Zyl decomposition relating to asymmetric scattering are dealt with in (Bhattacharaya and Touzi 2011), and the single/double bounce dichotomy for full pol covariance matrices in (Cui et al. 2014). In this paper these

CONTACT Allan A. Nielsen. Email: alan@dtu.dk. ORCID 0000-0002-4837-9449.

issues are not addressed further.

The data used here to illustrate the decompositions are X-band data from the F-SAR system (Reigber et al. 2013) from the German Aerospace Center (DLR) covering a small area in western Denmark.

2. Multilook polarimetric SAR data

In the covariance matrix formulation of multilook polarimetric SAR (polSAR) image data each pixel is described by a complex 3×3 matrix

$$\boldsymbol{C} = \begin{bmatrix} \langle S_{hh}S_{hh}^*\rangle & \sqrt{2}\langle S_{hh}S_{hv}^*\rangle & \langle S_{hh}S_{vv}^*\rangle \\ \sqrt{2}\langle S_{hv}S_{hh}^*\rangle & 2\langle S_{hv}S_{hv}^*\rangle & \sqrt{2}\langle S_{hv}S_{vv}^*\rangle \\ \langle S_{vv}S_{hh}^*\rangle & \sqrt{2}\langle S_{vv}S_{hv}^*\rangle & \langle S_{vv}S_{vv}^*\rangle \end{bmatrix}.$$

This matrix is Hermitian also known as self-adjoint, i.e., the matrix is equal to its own conjugate transpose, $\boldsymbol{C} = \boldsymbol{C}^H$, the superscript ^{H} denotes transpose and complex conjugate (which is denoted by *), $\langle\rangle$ denotes ensemble averaging. The trace, the determinant and all eigenvalues are real and nonnegative.

The general spectral decomposition of this matrix is

$$\boldsymbol{C} = \lambda_1\boldsymbol{e}_1\boldsymbol{e}_1^H + \lambda_2\boldsymbol{e}_2\boldsymbol{e}_2^H + \lambda_3\boldsymbol{e}_3\boldsymbol{e}_3^H$$

where λ_i are the eigenvalues of $\boldsymbol{C}$ and $\boldsymbol{e}_i$ the corresponding mutually orthogonal eigenvectors.

3. Eigenvalues and -vectors

In this section we solve the eigenvalue problem for the reflection symmetry case. For (fast) calculation of eigenvalues in the full/quad pol case we refer to (Uspensky 1948; Nielsen 2020; Cloude and Pottier 1997; Lee et al. 1999).

3.1. *Reflection Symmetry*

With the notation from (van Zyl 1993; van Zyl et al. 2011) the reflection symmetry version of the covariance matrix is

$$\boldsymbol{C}_r = \begin{bmatrix} \xi & 0 & \rho \\ 0 & \eta & 0 \\ \rho^* & 0 & \zeta \end{bmatrix}.$$

The eigenvalues $\lambda_i, i = 1, 2, 3$ are found by solving

$$(\xi - \lambda_i)(\eta - \lambda_i)(\zeta - \lambda_i) - (\eta - \lambda_i)|\rho|^2 = 0$$

leading to

$$\begin{aligned}\lambda_{1,2} &= \frac{\zeta+\xi\pm\sqrt{\Delta}}{2}\\ \lambda_3 &= \eta,\end{aligned}$$

where $\Delta=(\zeta-\xi)^2+4|\rho|^2$ ($\Delta\geq 0$) and $\lambda_1\geq\lambda_2$.

The first and second eigenvalues are both associated with either single bounce scattering (odd number of reflections) or double bounce scattering (even number of reflections), see (1). The third eigenvalue is the covariance matrix element $\eta=2\langle S_{hv}S_{hv}^*\rangle$ associated with the remainder, often volume scattering in vegetation or dihedrals rotated with respect to the flight line. Circular polarization to avoid the rotation dependency and determination of the rotation angle are described in (Lee et al. 2002; Yamaguchi et al. 2011). In (Yamaguchi et al. 2011) the angle is determined by cross-polarization minimization. Neither issue is pursued further here.

With

$$\begin{aligned}\Lambda_1 &= \lambda_1\frac{[\zeta-\xi+\sqrt{\Delta}]^2}{[\zeta-\xi+\sqrt{\Delta}]^2+4|\rho|^2}\\ \Lambda_2 &= \lambda_2\frac{[\zeta-\xi-\sqrt{\Delta}]^2}{[\zeta-\xi-\sqrt{\Delta}]^2+4|\rho|^2}\\ \Lambda_3 &= \lambda_3\\ \alpha_v &= \frac{2\rho}{\zeta-\xi+\sqrt{\Delta}}\\ \beta_v &= \frac{2\rho}{\zeta-\xi-\sqrt{\Delta}},\end{aligned}$$

we have the corresponding eigenvectors, see (van Zyl 1993; van Zyl et al. 2011)

$$\begin{aligned}\boldsymbol{e}_1 &= \sqrt{\frac{[\zeta-\xi+\sqrt{\Delta}]^2}{[\zeta-\xi+\sqrt{\Delta}]^2+4|\rho|^2}}\begin{bmatrix}\alpha_v\\0\\1\end{bmatrix}\\ \boldsymbol{e}_2 &= \sqrt{\frac{[\zeta-\xi-\sqrt{\Delta}]^2}{[\zeta-\xi-\sqrt{\Delta}]^2+4|\rho|^2}}\begin{bmatrix}\beta_v\\0\\1\end{bmatrix}\\ \boldsymbol{e}_3 &= \begin{bmatrix}0\\1\\0\end{bmatrix}.\end{aligned}$$

For $\boldsymbol{e}_3$ we could choose any complex vector with first and third components equal to zero and second component on the unit circle in the complex plane. As in (van Zyl 1993; van Zyl et al. 2011) we choose 1. Incidentally, each $\boldsymbol{e}_i$ has arbitrary complex phase $\exp(j\phi_i)$.

For $|\rho|>0$ the denominator of α_v is positive and the denominator of β_v is negative. Also, $\alpha_v\beta_v^*=\alpha_v^*\beta_v=-1$ (leading to $\boldsymbol{e}_1^H\boldsymbol{e}_2=0$; trivially $\boldsymbol{e}_1^H\boldsymbol{e}_3=\boldsymbol{e}_2^H\boldsymbol{e}_3=0$) and since

for any complex number z, $1/z = z^*/|z|^2$ we have the relations

$$\beta_v = -\frac{1}{\alpha_v^*} = -\frac{\alpha_v}{|\alpha_v|^2} \quad \text{and} \quad |\beta_v|^2 = \frac{1}{|\alpha_v|^2}.$$

This leads to the decomposition

$$\begin{aligned} \boldsymbol{C}_r &= \lambda_1 \boldsymbol{e}_1 \boldsymbol{e}_1^H + \lambda_2 \boldsymbol{e}_2 \boldsymbol{e}_2^H + \lambda_3 \boldsymbol{e}_3 \boldsymbol{e}_3^H \\ &= \Lambda_1 \begin{bmatrix} |\alpha_v|^2 & 0 & \alpha_v \\ 0 & 0 & 0 \\ \alpha_v^* & 0 & 1 \end{bmatrix} + \Lambda_2 \begin{bmatrix} |\beta_v|^2 & 0 & \beta_v \\ 0 & 0 & 0 \\ \beta_v^* & 0 & 1 \end{bmatrix} + \\ &\quad \Lambda_3 \begin{bmatrix} 0 & 0 & 0 \\ 0 & 1 & 0 \\ 0 & 0 & 0 \end{bmatrix}. \end{aligned} \tag{1}$$

To explicitly distinguish between single and double bounce scattering, we sort the above parameters such that

- λ_1, $\boldsymbol{e}_1$, Λ_1 and α_v more closely represent single bounce scattering (the argument of $\rho = \langle S_{hh} S_{vv}^* \rangle$ is closer to 0 than to $\pm\pi$ which means that the real part of ρ is nonnegative), and
- λ_2, $\boldsymbol{e}_2$, Λ_2, and β_v more closely represent double bounce scattering (the argument of $\rho = \langle S_{hh} S_{vv}^* \rangle$ is closer to $\pm\pi$ than to 0 which means that the real part of ρ is negative).

As a measure of target disorder, entropy H is defined as

$$H = -\sum_{i=1}^{3} p_i \log_3 p_i \quad \text{with} \quad p_i = \frac{\lambda_i}{\sum_{i=1}^{3} \lambda_i},$$

$0 \leq H \leq 1$. Low entropy is associated with a single dominant scattering mechanism, high entropy with random scattering.

A good RGB visualization of the decomposition is

- red: double bounce scattering given by
  $\lambda_2 = \Lambda_2(|\beta_v|^2+1)$; $|\beta_v|^2+1$ is the trace of the second matrix in the decomposition of $\boldsymbol{C}_r$ in (1),
- green: volume scattering given by $\lambda_3 = \Lambda_3$,
- blue: single bounce scattering given by
  $\lambda_1 = \Lambda_1(|\alpha_v|^2+1)$; $|\alpha_v|^2+1$ is the trace of the first matrix in the decomposition of $\boldsymbol{C}_r$ in (1).

If one is less interested in the strongly reflecting man-made objects in the scene but more interested in overall structure, the RGB visualization can be made by means of square roots or logarithms of the eigenvalues. This will enhance the visual impression of the weaker reflectors.

3.2. *Full/Quad Pol*

For full/quad pol we have the full covariance matrix

$$\boldsymbol{C} = \begin{bmatrix} \xi & a & \rho \\ a^* & \eta & b \\ \rho^* & b^* & \zeta \end{bmatrix}$$

and the eigenvalues are found as described in (Uspensky 1948; Nielsen 2020). The solutions given in (Nielsen 2020) are well suited for fast array based computer implementation.

In this full/quad pol case the third eigenvalue, λ_3, is the one closest to $\eta = 2\langle S_{hv} S_{hv}^* \rangle$. Again, we sort the remaining two eigenvalues λ_1 and λ_2 according to the sign of the real part of $\rho = \langle S_{hh} S_{vv}^* \rangle$, i.e., according to whether the argument of ρ is closer to 0 or to $\pm\pi$.

One could argue that in the full/quad pol case unlike in the reflection symmetry case, the eigenvectors do not have direct interpretations as being associated with specific scattering mechanisms (single bounce, double bounce, volume scattering). On the other hand the Cloude/van Zyl decomposition for reflection symmetric data places restrictions on the data *before* the decomposition—especially, man-made objects certainly do not exhibit reflection symmetry—whereas what we do here challenges the interpretation *after* the decomposition.

To facilitate the interpretation of the scattering mechanism in this full matrix case we use the $\bar{\alpha}$ angle suggested by Cloude and Pottier (Cloude and Pottier 1997; Lee et al. 1999). $\bar{\alpha}$ is calculated from the eigenvectors of the coherency matrix (we reuse the symbol $\boldsymbol{e}_i, i = 1, 2, 3$ for eigenvectors)

$$\boldsymbol{e}_i = \exp(j\phi_i) \begin{bmatrix} \cos\alpha_i \\ \sin\alpha_i \cos\beta_i \exp(j\delta_i) \\ \sin\alpha_i \sin\beta_i \exp(j\gamma_i) \end{bmatrix}$$

where α_i, β_i, δ_i and γ_i are angles which characterize the scattering. Here we are interested in the α_i only. For the first element e_{i1} of $\boldsymbol{e}_i$ we have

$$\begin{aligned} |e_{i1}|^2 &= e_{i1} e_{i1}^* \\ &= \exp(j\phi_i) \cos\alpha_i \exp(-j\phi_i) \cos\alpha_i \\ &= \cos^2\alpha_i \end{aligned}$$

and therefore

$$\alpha_i = \arccos|e_{i1}|$$

(arccos is sometimes written as $\cos^{-1}$). For $\bar{\alpha}$ we have

$$\bar{\alpha} = \sum_{i=1}^{3} p_i \alpha_i$$

with the p_i calculated as in the above subsection 3.1 but now based on the eigenvalues of the full matrix (the full covariance matrix and the coherency matrix have the same

Figure 1. Part of Vejers, Denmark, approximately the area covered by the F-SAR data, from Google Earth. We see summer houses, caravan sites with a swimming pool and service buildings (a grocery store, a petrol station etc.), the main road called Vejers Havvej (where the text "Vejers" appears) going mostly east-west, dirt roads, vegetation etc. Note the two red circles in the left part of the image, top-center (near a swimming pool) and bottom (a big house).

eigenvalues). Alternatively, the α_i may be calculated by means of the eigenvector-eigenvalue identity where we obtain the $|e_{i1}|^2$ without calculating $\boldsymbol{e}_i$ (Hensley 2021; Denton et al. 2022; Nielsen 2022). This speeds up calculations immensely compared to calls to built-in eigensolvers in for-loops over rows an columns, see (Nielsen 2022). For $\bar{\alpha}$ we have

- $\bar{\alpha} = 0°$ is associated with single bounce (surface) scattering,
- $\bar{\alpha} = 45°$ with scattering from differently oriented dipoles (typically vegetation or dihedral targets rotated with respect to the flight line), and
- $\bar{\alpha} = 90°$ with (conductive) double bounce scattering.

4. Data example

In a project headed by the Danish Ministry of Defence Acquisition and Logistics Organization (DALO) the F-SAR system of the German Aerospace Center (DLR) has been used to acquire data at several locations in Denmark and Greenland. The F-SAR offers the possibility of exploring the performance of a high resolution, fully polarimetric SAR system with five frequency bands in the range ∼300 MHz to ∼10 GHz (Reigber et al. 2013).

The decompositions are illustrated with airborne F-SAR X-band data (frequency

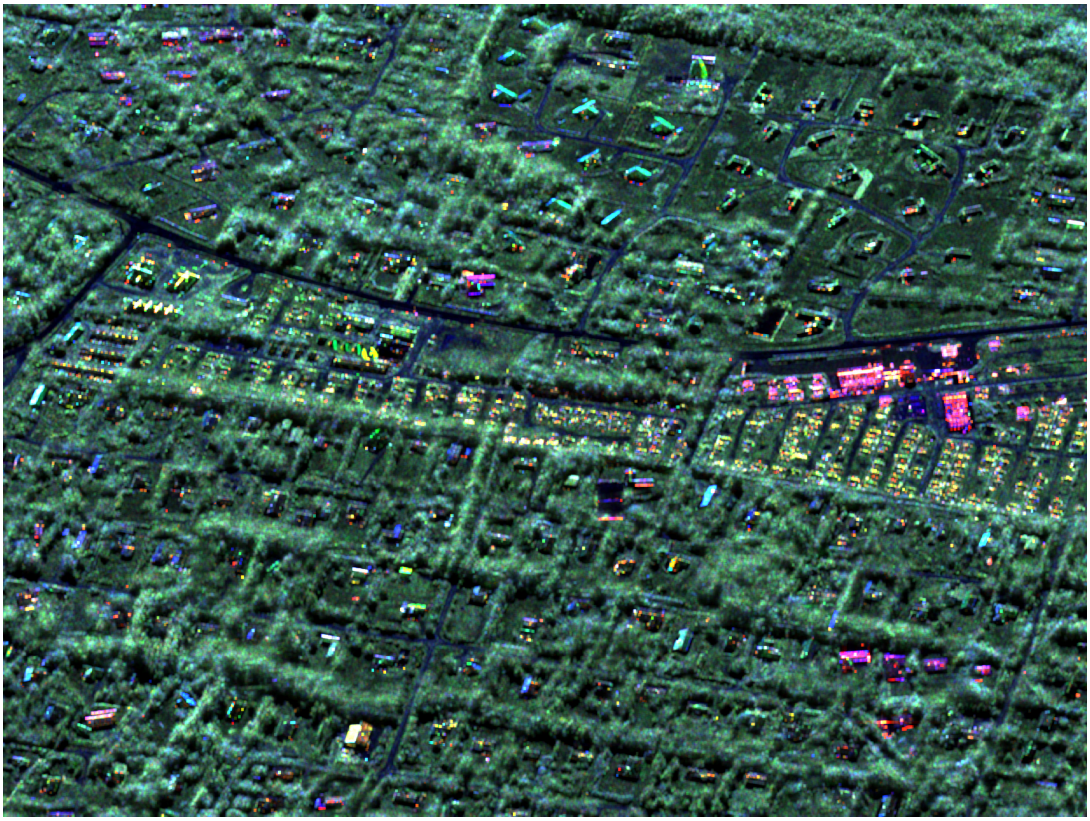

Figure 2. Original reflection symmetry based Cloude/van Zyl decomposition. Red is $\sqrt{\lambda_2}$ (double bounce scattering or even number of reflections), green is $\sqrt{\lambda_3}$ (volume scattering), blue is $\sqrt{\lambda_1}$ (single bounce scattering or odd number of reflections).

9.60 GHz corresponding to a wavelength of ∼3 cm). The data were acquired on 20 June 2017 covering a central part of the village Vejers on the Danish west coast, Figure 1. The scene covers the east-west main road (called Vejers Havvej where the text "Vejers" appears in Figure 1 and depicted in black in Figures 2 and 3) going to and from the sea, camp sites with caravans to the south of the road, a swimming pool, parking lots and several service buildings (grocery store, petrol station etc.) as well as many small and big houses north and south of the road. Note the two red circles.

In Figures 2 and 3 in which square roots of the eigenvalues are shown as RGB, red objects are mainly buildings which are characterized by double bounce reflection. Green objects in the two images are mainly characterized by volume scattering typically vegetation or dihedral targets which are rotated with respect to the flight line. Blue areas in the two images are objects which are characterized by single bounce reflection. Magenta is a mix of red and blue and therefore magenta objects represent a combination of double and single bounce reflection. Yellow is a mix of red and green and therefore yellow objects represent a combination of double bounce reflection and volume scattering. Cyan is a mix of green and blue and therefore cyan objects represent a combination of volume scattering and single bounce reflection. White and gray objects represent a combination of all three types of scattering.

In a few places differences between the two decompositions can be seen (two examples are marked by red circles in Figure 1). For example a large whitish trapezoid-shaped roof of the circled building to the bottom-left in Figure 2 appears more yellow in Figure 3. This means that our version of the decomposition suggests two scattering

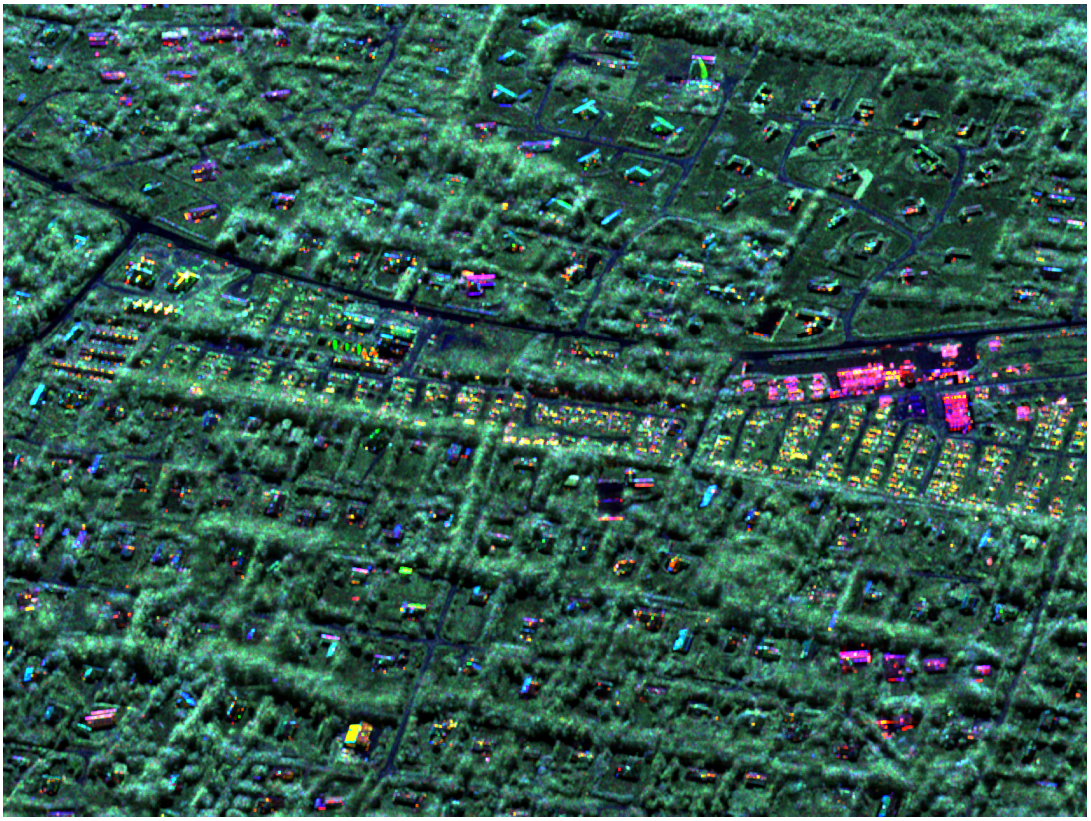

Figure 3. Full/quad pol version of Cloude/van Zyl decomposition. Red is $\sqrt{\lambda_2}$, green is $\sqrt{\lambda_3}$, blue is $\sqrt{\lambda_1}$. A few differences from Figure 2 can be seen for some strong scatterers, see text and Figure 4.

mechanisms as opposed to three for the original one. Also, two yellow building parts (also circled) just south of Vejers Havvej in the middle-left part of Figure 2 immediately left of the swimming pool seen in Figure 1 are red in Figure 3. This means that our version of the decomposition suggests one scattering mechanism as opposed to two for the original one. Similar considerations are valid also for other targets not mentioned here.

Figure 4 shows the difference between entropies as obtained by the original and the full matrix version of the decomposition. Differences are consistently nonnegative (the minimum value is 0.00, the maximum value is 0.62) and large differences are on bright man-made objects (houses, caravans etc.). This means that the suggested full matrix version gives less target scattering mechanism disorder, i.e., better scattering description for these objects.

Figure 5 shows eigenvalues for the two versions of the van Zyl decomposition for two different situations: a road pixel (left) and a pixel on the roof of the circled house (right), original version for reflection symmetry in red, our version for the full covariance matrix in blue. For the road the eigenvalues are very similar. For the house, unlike the case for the original decomposition, we get one dominant scattering mechanism and hence less scattering mechanism disorder for our version.

Table 1 shows $\bar{\alpha}$ for a few selected pixels in Figure 3 including the two circled targets in Figure 1. Correspondence with the expected values for different scattering mechanisms mentioned in Section 3.2 is satisfactory. Specifically, we see that the circled big house for our version exhibits the expected double bounce scattering.

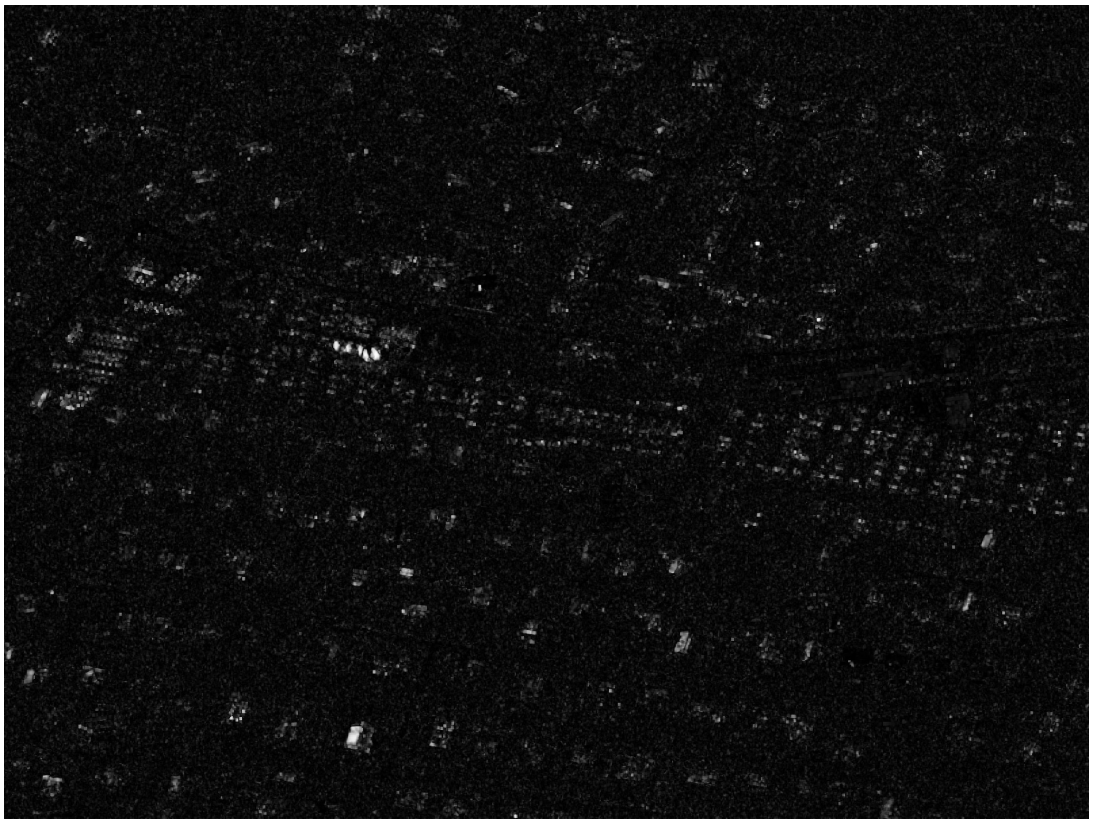

Figure 4. Entropy (in the interval $[0, 1]$) for the original reflection symmetry decomposition minus entropy ($[0, 1]$) for the full/quad pol version. Differences are consistently nonnegative, i.e, we always have lower entropy for the full/quad pol version. Large differences (up to 0.62) are concentrated on bright man-made objects (houses, caravans etc.). Hence the suggested version gives less target scattering mechanism disorder for these objects.

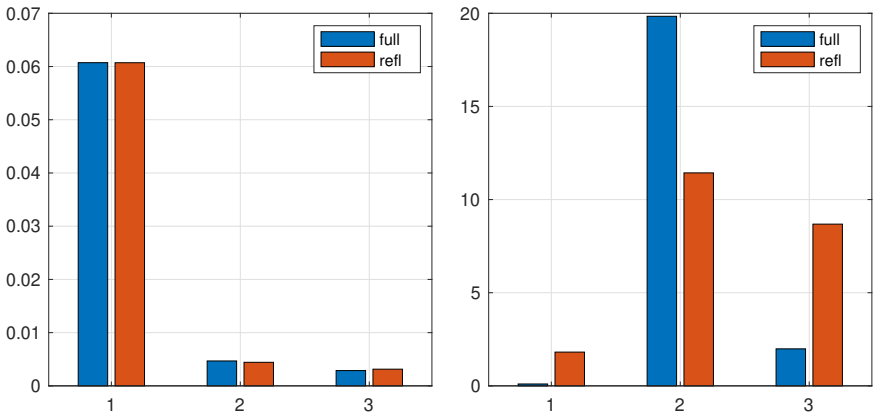

Figure 5. Eigenvalues for the Cloude/van Zyl decomposition, original version for reflection symmetry in red, our version for the full covariance matrix in blue. For the original version "1" represents single bounce, "2" double bounce and "3" volume scattering. The left figure shows eigenvalues for a (very low backscatter) road pixel where the two sets of eigenvalues are very similar. Contrary to this the right figure shows eigenvalues for a (high backscatter) pixel on the roof of the circled house where the two sets are very different. Note the very different scales on the two y-axes.

Table 1. $\bar{\alpha}$ for a few selected pixels in Figure 3.

	$\bar{\alpha}$
Big house (circled)	68°
West of swimming pool (circled)	62°
Wood	30°
Road	11°

5. Conclusions

We propose a version of the Cloude/van Zyl decomposition for full/quad pol synthetic aperture radar data. The Cloude/van Zyl decomposition for reflection symmetric data offers direct interpretation of the eigenvectors as being associated with single bounce, double bounce or volume scattering but places restrictions on the data before the decomposition, especially, man-made objects certainly do not exhibit reflection symmetry. Contrary to this, since the eigenvectors in the full/quad pol case do not have direct interpretations as being associated with the same specific scattering mechanisms, what we do here challenges the interpretation after the decomposition. To facilitate interpretation of the scattering mechanism in this case we use the $\bar{\alpha}$ angle.

The explicit distinction between single and double bounce targets in the original reflection symmetry Cloude/van Zyl decomposition obtained by sorting the first two eigenvalues according to whether the phase of $\langle S_{hh}S_{vv}^{*}\rangle$ is closer to 0 or to $\pm\pi$, is retained in this full/quad pol version.

In the case given, differences between our version and the original decomposition based on reflection symmetry occur especially for bright, man-made objects. With our version these objects have consistently lower entropy. Hence the suggested version gives less target scattering mechanism disorder for these objects. This is depicted also in the visualizations shown, e.g., white objects for reflection symmetry to yellow objects for full/quad pol, or yellow to red objects.

Matlab code for calculating eigenvalues and entropy for the two decompositions, and their visualization is available on the first author's homepage https://people.compute.dtu.dk/alan/ under "Publications".

References

Bhattacharaya, A. and R. Touzi (2011). Polarimetric SAR urban classification using the Touzi target scattering decomposition. *Canadian Journal of Remote Sensing 37*(4), 323–332. https://doi.org/10.5589/m11-042.

Cloude, S. R. (1992). Uniqueness of target decomposition theorems in radar polarimetry. In *Direct and Inverse Methods in Radar Polarimetry, Part I, NATO Advanced Science Institutes Series*, pp. 267–296. (Event Bad Windsheim, Germany, 18-24 September 1988).

Cloude, S. R. and E. Pottier (1997, Jan.). An entropy based classification scheme for land applications of polarimetric SAR. *IEEE Transactions on Geoscience and Remote Sensing 35*(1), 68–78. https://doi.org/10.1109/36.551935.

Cui, Y., Y. Yamaguchi, J. Yang, H. Kobayashi, P. S.-E, and G. Singh (2014, Apr.). On complete model-based decomposition of polarimetric SAR coherency matrix data. *IEEE Transactions on Geoscience and Remote Sensing 52*(4), 1991–2001. https://doi.org/10.1109/TGRS.2013.2257603.

Denton, P. B., S. J. Parke, T. Tao, and X. Zhang (2022, Jan.). Eigenvectors from eigenvalues:

A survey of a basic identity in linear algebra. *Bulletin of the American Mathematical Sociey 59*(1), 31–58. https://doi.org/10.1090/bull/1722.

Freeman, A. and S. L. Durden (1998, May). A three-component scattering model for polarimetric SAR data. *IEEE Transactions on Geoscience and Remote Sensing 36*(3), 963–973. https://doi.org/10.1109/36.673687.

Hensley, S. (2021, Jul.). The eigenvector-eigenvalue identity and radar polarimetry. In *IEEE International Geoscience and Remote Sensing Symposium (IGARSS)*, Brussels, Belgium, pp. 2–5. https://doi.org/10.1109/IGARSS47720.2021.9554916.

Lee, J.-S., M. R. Grunes, T. L. Ainsworth, L.-J. Du, D. L. Schuler, and S. R. Cloude (1999, Sep.). Unsupervised classification using polarimetric decomposition and the complex Wishart classifier. *IEEE Transactions on Geoscience and Remote Sensing 37*(5), 2249–2258. https://doi.org/10.1109/36.789621.

Lee, J.-S., D. L. Schuler, T. L. Ainsworth, E. Krogager, D. Kasilingam, and W.-M. Boerner (2002, Jan.). On the estimation of radar polarization orientation shifts induced by terrain slopes. *IEEE Transactions on Geoscience and Remote Sensing 40*(1), 30–41. https://doi.org/10.1109/36.981347.

Nielsen, A. A. (2020, Oct.). Fast matrix based computation of eigenvalues and the Loewner order in polSAR data. *IEEE Geoscience and Remote Sensing Letters 17*(10), 1727–1731. https://doi.org/10.1109/LGRS.2019.2952202 and https://www2.imm.dtu.dk/pubdb/p.php?7151.

Nielsen, A. A. (2022, Apr.). The eigenvector-eigenvalue identity applied to fast calculation of polSAR scattering characterization. *IEEE Geoscience and Remote Sensing Letters (Early Access)*.

Reigber, A., R. Scheiber, M. J. ager, P. Prats-Iraola, I. Hajnsek, T. Jagdhuber, K. P. Papathanassiou, M. Nannini, E. Aguilera, S. Baumgartner, R. Horn, A. Nottensteiner, and A. Moreira (2013, Mar.). Very-high resolution airborne synthetic aperture radar imaging: Signal processing and applications. *Proceedings of the IEEE 101*(3), 759–783. https://doi.org/10.1109/JPROC.2012.2220511.

Uspensky, J. V. (1948). *Theory of Equations*. McGraw Hill.

van Zyl, J. J. (1993). Application of Cloude's target decomposition theorem to polarimetric imaging radar data. In *Proceedings of SPIE 1748, Radar Polarimetry*, pp. 184–191. https://doi.org/10.1117/12.140615, (Event San Diego, USA, 1992).

van Zyl, J. J., M. Arii, and Y. Kim (2011, Sep.). Model-based decomposition of polarimetric SAR covariance matrices constrained for nonnegative eigenvalues. *IEEE Transactions on Geoscience and Remote Sensing 49*(9), 3452–3459. https://doi.org/10.1109/TGRS.2011.2128325.

Yamaguchi, Y., A. Sato, W.-M. Boerner, R. Sato, and H. Yamada (2011, Jun.). Four component scattering power decomposition with rotation of coherency matrix. *IEEE Transactions on Geoscience and Remote Sensing 49*(6), 2251–2258. https://doi.org/10.1109/TGRS.2010.2099124.